Journal of Molecular Structure 1237 (2021) 130282

Contents lists available at ScienceDirect

Journal of Molecular Structure

journal homepage: www.elsevier.com/locate/molstr

Synthesis, structure analysis, DFT calculations, Hirshfeld surface studies, and energy frameworks of 6-Chloro-3-[(4-chloro-3-methylphenoxy)methyl][1,2,4]triazolo[4,3-b]pyridazine

Hamdi Hamid Sallam[a,b], Yasser Hussien Eissa Mohammed[c,d], Fares Hezam Al-Ostoot[c,e], M.A. Sridhar[a,*], Shaukath Ara Khanum[c]

[a] Department of Studies in Physics, Manasagangotri, University of Mysore, Mysuru, 570 006, India
[b] Department of Physics, Faculty of Education and Science, Turba Branch, Taiz University, Yemen
[c] Department of Chemistry, Yuvaraja's College, University of Mysore, Mysuru 570 006, India
[d] Department of Biochemistry, Faculty of Applied Science, University of Hajjah, Yemen
[e] Department of Biochemistry, Faculty of Education and Science, Al-Baydha University, Yemen

ARTICLE INFO

Article history:
Received 21 December 2020
Revised 2 March 2021
Accepted 10 March 2021
Available online 15 March 2021

Keywords:
Synthesis
Triazolo[4,3-b]pyridazine
XRD
DFT calculations
Hirshfeld surface
energy framework

ABSTRACT

In medicinal chemistry, heterocyclic compounds like pyridazine analogs has shown significant pharmaceutical importance. In this view, the compound 6-chloro-3-[(4-chloro-3-methylphenoxy) methyl][1,2,4]triazolo[4,3-b]pyridazine (**4**) was synthesized treating 2-(4-chloro-3 methylphenoxy) acetic acid (**1**) with 3-chloro-6-hydrazinylpyridazine (**2**) in dry dichloromethane (DCM) followed by the addition of lutidine, and *O*-(benzotriazole-1-yl)-*N*,*N*,*N*',*N*'-tetramethyluronium tetrafluoroborate (TBTU) in cold condition to achieve *2-(4*-chloro-3-methylphenoxy)-*N*'-(4-chloropyridazin-3-yl)acetohydrazide (**3**). Then the compound (**3**) was heated with chloroamine T in the presence of ethanol to furnish the desired compound (**4**). The synthesized compound was elucidated by spectroscopic techniques (IR, NMR and LC-MS), and finally the structure was confirmed by XRD technique. The compound (**4**) has crystallized in the monoclinic crystal system with the space group $P2_1/c$. Density functional theory calculations were carried out to find the extent of harmony between the theoretical and experimental values. HOMO-LUMO energy gap and the global reactivity descriptor values of the compound (**4**) have been determined. In the structure C-H...N intermolecular hydrogen bond and the scarce C-Cl...cg interaction are observed. Hirshfeld surface analysis is also performed. Energy frameworks were constructed to understand the packing of molecules by studying the different intermolecular interaction energies.

1. Introduction

Triazole, also known as pyrrodiazole is one of the essential azoheterocycles containing a five-membered ring and its derivatives are important structural moieties of several potential applications [1,2]. Due to its medicinally favored, triazole is commonly integrated into synthetic therapeutic agents and bioactive natural items [3]. Triazoles exhibit excellent electron-transport and hole-blocking properties because of their electron-deficient nature, causing them interesting organic materials in material science applications [4]. Pyridazines also known as (oizine or 1,2-diazine) are six-membered azoheterocylic compounds. In the field of medicinal and drug design, heterocyclic compounds based on the pyridazine skeleton have been reported as important biologically active pharmacophores, offering a wide variety of safe and potent drugs [5,6]. Therefore, the pyridazine ring is part of the structure of several marketable therapeutic agents, such as cadralazine and hydralazine, minaprine, pipofezine, etc [7,8]. Interestingly many pharmacological properties are endowed with triazole and pyridazine derivatives, in this connection researchers has integrated these two rings and identified them as antitubulin [9], anti-inflammatory, antibacterial [10], and anticonvulsant [11] agents and also as tyrosine kinase inhibitor [12]. In view of this, a number of synthetic procedures have been developed for the synthesis of 1,2,4-triazolo[4,3-b]pyridazine derivatives. Regrettably, most of these methods suffer from various disadvantages such as hazardous materials, longer reaction times at higher reaction temperatures and poor yield. Usefulness of chloramine T in oxidative transformation is a valuable approach for greener synthesis because of its easy availability, mild

* Corresponding author.
E-mail address: mas@physics.uni-mysore.ac.in (M.A. Sridhar).

https://doi.org/10.1016/j.molstruc.2021.130282
0022-2860/

reaction condition and ease of handling. With this background, a simple technique was developed in the present study for the synthesis of 6-chloro-3-[(4-chloro-3-methylphenoxy) methyl][1,2,4] triazolo[4,3-b] pyridazine (4) using chloramine T as an eco-friendly agent [13]. In view of their broad spectrum of biological properties and as a part of our ongoing work on synthesis and characterization of heterocyclic derivatives [14-16]. The compound was synthesized and characterized spectroscopically and the molecular structure was confirmed by single crystal X-ray diffraction studies. The density functional theory calculations for the title compound were carried out to compare the theoretical and experimental results.

2. Experimental details

2.1. Materials and methods

The chemicals required for the synthesis of title compound (4-Chlorophenol, Ethyl chloroacetate, 3-chloro-6-hydrazinylpyridazine, TBTU) were procured from Sigma Aldrich Chemical Co. The progress of the reaction was monitored by Thin Layer Chromatography (TLC) performed on aluminium-backed silica plates, and the spots were detected by exposure to UV-lamp at λ= 254 nm. Melting point and boiling point were measured on a Chemiline, microcontroller based melting point/boiling point-Cl725 apparatus with a digital thermometer. IR spectra were recorded on the Agilent Technologies Cary 630 FT-IR spectrometer. ^{1}H and ^{13}C NMR spectra were recorded on VNMRS-400 Agilent-NMR spectrophotometer. The mass spectra were obtained with a VG70-70H spectrometer. The elemental analysis (C, H, and N) was performed on Elementar Vario EL III elemental analyzer. The result of elemental analysis is within ±0.4% of the theoretical value.

2.2. 2-(4-chloro-3-methylphenoxy)-N'-(4-chloropyridazin-3-yl) acetohydrazide (3)

To a solution of 2-(4-chloro-3-methylphenoxy)acetic acid (**1**, 2 mmol) in dry DCM (20 ml), lutidine (3 mmol) was added at 25-27°C, followed by the addition of 3-chloro-6-hydrazinylpyridazine (**2**, 2 mmol). The reaction mixture was stirred at the same temperature for 35 minutes. After reducing the temperature to 0-5°C, TBTU (2 mmol) was added to the mixture. The temperature was maintained below 5°C for a period of 30 minutes and the reaction mass was stirred overnight. The solvent was evaporated under reduced pressure, quenched by the addition of crushed ice, and the solid obtained was filtered and dried. This crude product was subjected to column chromatography, and eluted with a solvent mixture of ethyl acetate: hexane (4:1) to get the pure product which was recrystallized to afford compound (**3**).

2.3. Synthetic procedure for 6-chloro-3-((4-chloro-3-methylphenoxy)methyl)-[1,2,4]triazolo [4,3-b]pyridazine (4)

The compound (**3**, 0.02 mol) and chloroamine T (2 mmol) in ethanol was heated and refluxed with stirring for 5 h. The sodium chloride formed in the reaction was filtered off, washed, and then evaporated in vacuum; the residue was extracted with 5% hydrochloric acid, and washed thoroughly with dichloromethane. The aqueous layer was neutralized with 10% sodium hydroxide to achieve compound (**4**).

2.4. Spectral data

2.4.1. 2-(4-chloro-3-methylphenoxy)-N'-(6-chloropyridazin-3-yl) acetohydrazide (3)

Yield 70%; M.P 133-135°C; FT-IR (KBr, ν_{max} cm^{-1}): 1660 (C=O), 3130-3240 (NH-NH); ^{1}H NMR (400 MHz, DMSO) δ (ppm): 2.35 (s, 3H, CH_3), 4.60 (s, 2H, OCH_2), 6.81-8.11 (m, 3H, Ar-H), 6.92-7.18 (m, 2H, pyridazin-H), 8.95 (s, 1H, NH), 10.94 (s, 1H, NH); ^{13}C NMR (100 MHz, DMSO) δ (ppm): 20.90, 68.25, 118.30, 120.85, 130.35, 131.05, 133.14, 152.40, 158.52, 165.04, 168.75; LC-MS *m/z* 328 [M+2] 330 [M+4]. Anal. Calcd. For $C_{13}H_{12}Cl_2N_4O_2$ (326): C, 47.73; H, 3.70; N, 17.13. Found: C, 47.70; H, 3.68; N, 17.10%.

2.4.2. 6-chloro-3-((4-chloro-3-methylphenoxy)methyl)-[1,2,4]triazolo[4,3-b]pyridazine (4)

Yield: 75%.M.P 125-127 °C; IR (KBr, ν_{max} cm^{-1}): 1345 (C=N), ^{1}H NMR (400 MHz, DMSO) δ (ppm): 2.33 (s, 3H, CH_3), 5.56 (s, 2H, OCH_2), 6.87-7.24 (m, 3H, Ar-H), 6.16-8.12 (m, 2H, pyridazin-H). ^{13}C NMR (100 MHz, DMSO) δ (ppm): 20.85, 67.72, 118.05, 126.40, 128.20, 130.30, 133.98, 143.75, 154.50, 157.80, 165.20; LC-MS *m/z* 310 (M+2), 312 (M+4). Anal. Cal. For $C_{13}H_{10}Cl_2N_4O$ (308): C, 50.51; H, 3.26; N, 18.12. Found C, 50.50; H, 3.25; N, 18.10%.

2.5. X-ray crystallography

A block of brown coloured single crystal with approximate dimensions 0.12 × 0.15 × 0.10 mm^3 was selected for X-ray data collection. The X-ray intensity data were collected on a Bruker CMOS diffractometer equipped with MoK_α radiation with a wavelength 0.71073 Å [17]. The data reduction of all the measured reflections was done using Bruker *SAINT* [18] software package. Data were corrected for absorption effects using the multi-scan method. The crystal structure was solved using direct methods by employing *SHELXS*-97 and the refinement against F^2 was carried out using *SHELXL-18* [19]. Using *PLATON* [20], the geometrical calculations were carried out and the crystal graphics were generated by *MERCURY* [21] softwere. A total of 182 parameters were refined with 5080 unique reflections. The residual factor and the goodness of fit are 0.0575 and 1.035 respectively. The compound has CCDC No. 1881936 at the Cambridge Crystallographic Data Centre where full crystallographic data (CIF) has been deposited. Table 1 lists the crystal data collection and refinement details.

Table 1
The crystal data and structure refinement details.

Parameter	Value
Empirical formula	C_{13} H_{10} Cl_2 N_4 O_1
Formula weight	309.15
Temperature	293 K
Wavelength	0.71073 Å
θ range	3.33 ° to 33.29 °
Crystal system, Space group	Monoclinic, $P2_1/c$
Cell parameters	a = 6.1277(2) Å b = 20.7092(7) Å c = 10.4574(4) Å β = 90.414(2)°
Volume	1327.01(8) Å^3
Z	4
Density(calculated)	1.547 Mg m^{-3}
Absorption coefficient	0.489 mm^{-1}
F_{000}	632
Crystal size	0.12 mm × 0.15 mm × 0.10 mm
Index ranges	$-9 \le h \le 9$ $-31 \le k \le 31$ $-15 \le l \le 16$
Reflections collected	51919
Independent reflections	5080 [R_{int} = 0.0458]
Absorption correction	Multi-scan
Refinement method	Full matrix least-squares on F^2
Data / restraints / parameters	5080 / 0 / 182
Goodness-of-fit *on* F^2	1.039
Final [$I > 2\sigma(I)$]	R1 = 0.0575, wR_2 = 0.1168
R indices (all data)	R1 = 0.1056, wR_2 = 0.1366
Largest diff. peak and hole	0.370 and −0.432 e Å^{-3}

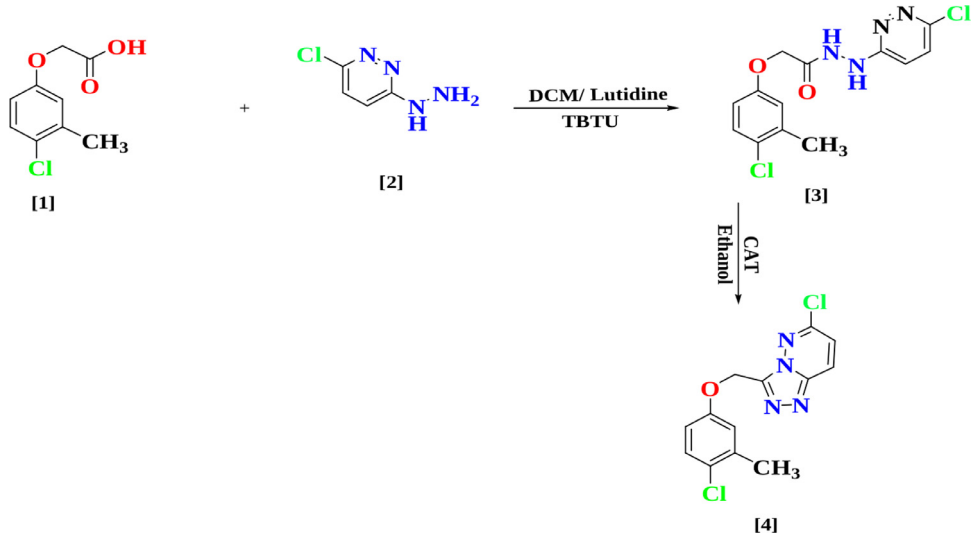

Fig. 1. Reaction pathway for the synthesis of the title compound (**4**).

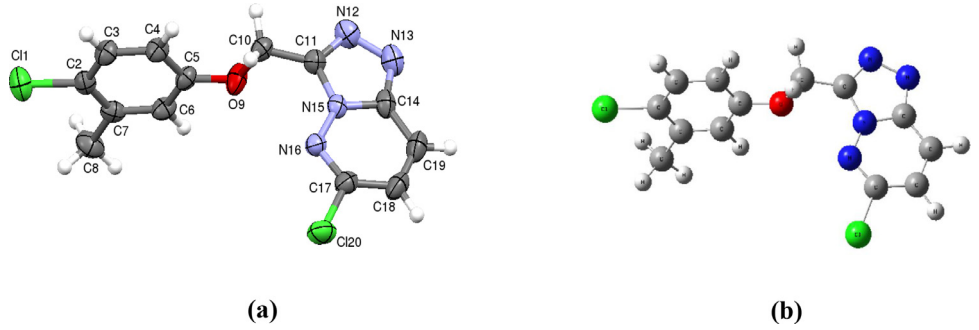

Fig. 2. a) ORTEP of the compound with thermal ellipsoids drawn at 50% probability. b) The optimized structure of the compound.

3. Results and discussions

3.1. Synthesis

Initially 2-(4-chloro-3-methylphenoxy)acetic acid (**1**), was treated with 3-chloro-6 hydrazinylpyridazine (**2**), in dry DCM followed by the addition of lutidine, and TBTU in cold condition to achieve 2-(4-chloro-3-methylphenoxy)-*N'*-(4-chloropyridazin-3-yl)acetohydrazide (**3**). Finally compound (**3**) and chloroamine T in ethanol were heated to obtain the title compound (**4**) as shown in Figure 1. The structure of the newly synthesized compound was assigned on the basis of FT-IR, NMR and LC-MS spectroscopic data and also by C, H, and N analysis. The FT-IR spectrum of compound (**3**) had shown the disappearance of OH stretching band of compound (**1**) and NH_2 stretching band of compound (**2**). At the same time compound (**3**) shown the appearance of keto and (NH-NH) stretching bands at 1660 and 3130-3240 cm^{-1} respectively. Similarly the compound (**4**) was confirmed by the disappearance of keto and (NH-NH) stretching bands of compound (**2**) and appearance of (C=N) band at 1345 cm^{-1}. The ^1H NMR spectrum of compound (**3**) has shown the disappearance of OH and NH_2 protons of compounds (**1**) and (**2**) respectively, and appearance of two NH groups' protons at δ 8.95 and 10.94. Finally, the compound (**4**) was confirmed by disappearance of two NH groups' protons of compound (3) (see Figure 1 in the supplementary file). Besides, the mass spectrum gave significant stable M+2 and M+4 peaks at *m/z* 310 and 312 respectively, which clearly affirmed the formation of compound (**4**).

3.2. XRD and DFT calculations

From the single crystal X-ray diffraction the 3D structure of the compond (**4**) has been confirmed. The compound crystallizes in the monoclinic crystal system with the space group $P2_1/c$. The unit cell constants are: a = 6.1277(2) Å, b = 20.7092(7) Å, c =10.4574(4) Å and β = 90.414(2)°. The *ORTEP* of the compound is shown in Figure 2(a). Using *Gaussian 09* package [22] with B3LYP function and 6-31G(d,p) basis set with the DMSO solvent, the density functional theory calculations were performed [23]. The optimized structure of the compound is shown in the Figure 2(b). The calculated bond lengths, bond angles and torsion angles of the compound are compared with the values obtained from single crystal X-ray diffraction. The calculated and experimental values are almost identical. Selected bond lengths, bond angles and torsion angles are listed in Table 2 (the full lists are given in Tables 1–3 of supplementary file).

3.3. HOMO and LUMO analyses

The frontier molecular orbitals (HOMO-LUMO) were investigated for the geometrically optimized structure. The molecular orbitals HOMO and LUMO of the compound are shown in Figure 3. The energy gap between HOMO (highest occupied molecular orbital) and LUMO (lowest unoccupied molecular orbital) describes the kinetic energy and chemical reactivity of the molecule. The small energy gap of the molecule implies a soft molecule with high chemical reactivity while, a large value of energy gap implies a hard molecule and low chemical reactivity [24]. For this

Table 2
Selected bond lengths, bond angles and torsion angles for the compound.

Atoms	Bond lengths (Å)			Bond lengths (Å)	
	XRD	DFT	Atoms	XRD	DFT
Cl1-C2	1.746(2)	1.7271	O9-C10	1.423(2)	1.4272
C2-C7	1.390(3)	1.3997	N15-C11	1.367(2)	1.3732
C7-C8	1.507(3)	1.5021	Cl20-C17	1.724(2)	Cl20-C17
Atoms	Bond angles (°)		**Atoms**	Bond angles (°)	
	XRD	**DFT**		**XRD**	**DFT**
C2-C7-C8	122.7(2)	122.08	N13-N12-C11	108.6(2)	108.14
C5-O9-C10	118.0(1)	117.14	N13-C14-C19	133.6(2)	132.58
C6-C7-C8	120.6(2)	120.49	Cl20-C17-C18	118.8(2)	118.78
Atoms	Torsion angles (°)		**Atoms**	Torsion angles (°)	
	XRD	**DFT**		**XRD**	**DFT**
Cl1-C2-C7-C6	179.2(1)	179.98	N15-N16-C17-C18	0.2(3)	0.39
C3-C4-C5-C6	0.1(3)	0.05	N15-C14-C19-C18	−0.7(3)	-0.64
O9-C10-C11-N15	−81.8(2)	-77.24	Cl20-C17-C18-C19	−178.9(2)	-179.3

Table 3
HOMO-LUMO and global reactivity descriptor values of the compound.

Parameter	Value
E_{HOMO}	-6.238 (eV)
E_{LUMO}	-2.768 (eV)
Energy gap (ΔE)	3.469 (eV)
Ionization potential (I)	6.238 (eV)
Electron affinity (A)	2.768 (eV)
Chemical hardness (η)	1.734 (eV)
Global softness (σ)	0.288 (eV^{-1})
Eletronegativity (X)	4.503 (eV)
Chemical potential (μ)	-4.503 (eV)
Eletrophilicity (ω)	5.845 (eV)

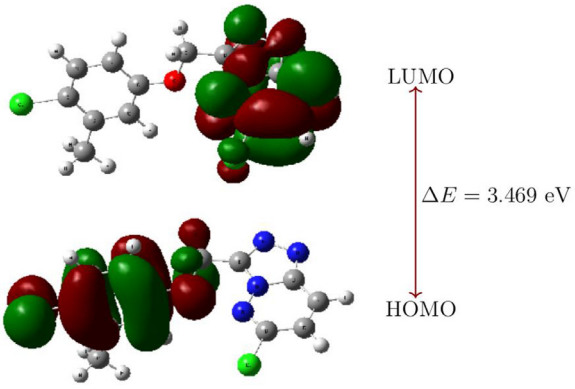

Fig. 3. HOMO-LUMO and energy gap of the title compound.

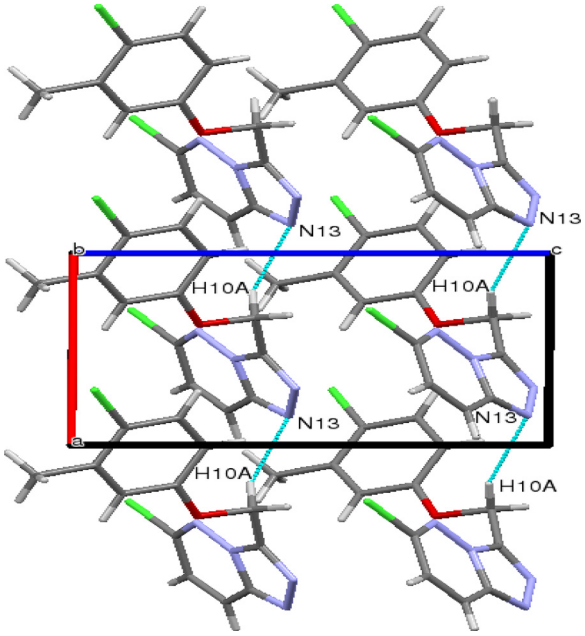

Fig. 4. The packing of the molecules viewed along *b* axis.

compound the HOMO and LUMO energies are -6.238 eV and -2.768 eV respectively. The energy gap between them is 3.469 eV, which referes to a soft molecule and easy transfer of electrons from HOMO to LUMO. The HOMO is localized in the phenoxy ring, oxygen atom and methylene, whereas the LUMO is localized in the triazole-pyridazine rings and chlorine atom. The energy gap and the other global reactivity descriptors for the compound were calculated (Table 3).

3.4. Description of structure

All the rings in the structure are sp^2 hybridized and are nearly planar. The maximum deviation from the plane for the triazole ring (C11-N12-N13-C14-N15) is 0.002 Å for C14; for the pyridazine ring (C14-N15-N16-C17-C18-C19) is 0.009 Å for N15; for the phenoxy ring (C2-C3-C4-C5-C6-C7) is 0.004 Å for C2; for the 9 membered ring (C11-N12-N13-C14-C19-C18-C17-N16-N15) is 0.013 Å for N13. The phenoxy ring deviates from the fused triazole-pyridazine ring system by a torsion angle value of 175.1(2)° for bridge atoms C5-O9-C10-C11. The chloro-methyl-phenoxy ring is not typical hexagonal. This distortion in the benzene ring is due to the chlorine atom and methyl group connected with it where the angles are greater than 120° at the points of substitution i.e., C3-C2-C7 = 122.5(2)° and C2-C7-C8 = 122.8(2)° respectively.

In the structure C10–H10A...N13 intermolecular hydrogen bond interactions (Table 4), that link the molecules into helical chains lying along *b* axis are presented in Figure 4. Additionally, as listed in Table 5 there are two C–Cl···Cg interactions, which is scarcely seen in the structure of organic molecules [25].

3.5. Hirshfeld surface analysis and fingerprint plots

CrystalExplorer-17 software [26] with B3LYP function and 6-31G (d, p) basis set was employed to generate the Hirshfeld surface and

Table 4
Hydrogen bonds geometry.

D-H ... A	D-H (Å)	H ... A (Å)	D ... A (Å)	D-H ... A (°)	Symmetry code
C10–H10A...N13	0.97	2.61	3.5247	157	*1+x,y,z*

Table 5
C–Cl···Cg interactions.

C-Cl...Cg	Cl -Cg (Å)	C..Cg (Å)	Gamma (°)	C-Cl ..Cg (°)	Symmetry codes
C17-Cl20... Cg(1)	3.5359(10)	4.157(2)	17.07	98.52(7)	*X,3/2-Y,-1/2+Z*
C2-Cl1...Cg (2)	3.8274(10)	5.1326(19)	27.22	130.33(7)	*-X,1/2+Y,3/2-Z*

Cg(1) is the centroid of the triazole ring and Cg(2) is the centroid of the pyridazine ring.

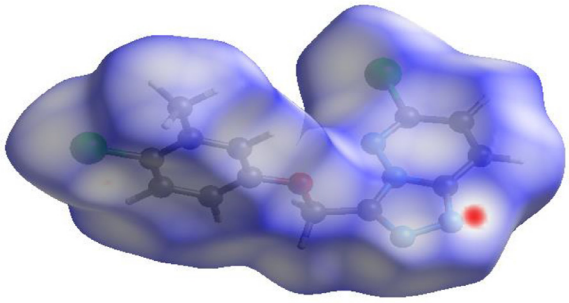

Fig. 5. Hirshfeld surface mapped over d_{norm}.

2D fingerprint plots of each type of contact in Hirshfeld surface area for the compound. The Hirshfeld surface volume and surface area are 324.88 Å^3 and 313.61 Å^2 respectively. The mapping of Hirshfeld surface over normalized contact distance d_{norm} is shown in Figure 5. This mapping shows blue, red, and white color schemes. The bright red region on it is due to C10–H10A...N13 intermolecular hydrogen bonds. The blue (d_{norm} is positive) and red (d_{norm} is negative) colored regions on the surface are from longer and shorter contacts than van der Waals radii respectively; the white colored regions represent the contacts which are equal to the van der Waals radii i.e, d_{norm} = zero [27].

The two-dimensional fingerprint plots enable us to know the percentage contribution of each type of contact to the total Hirshfeld surface area. Figure 6 shows the fingerprint plots of d_i (distance from the nearest atom internal to the surface), and d_e (distance from the nearest atom external to the surface). The strong intermolecular interactions appear as distinct spikes in the fingerprint plots. The decomposed fingerprint plot highlights the close contacts of a particular atom pair. Among all the contacts, N-H contacts contribute the most (22.0%) to the total Hirshfeld surface area. The two sharp peaks observed at the top left and bottom right of the plot are from the close intermolecular N-H contacts (Figure 6b). H-H contacts (Figure 6d) showed as a characteristic spike in the middle by contributing 18.4% to the total Hirshfeld surfaces. H-H and N-H interactions have significant contribution to the crystal packing where the distance $d_i + d_e \approx 2.2$ Å and 2.5 Å respectively (i.e., the distance is shorter than van der Waals radii). The wings in Figure 6e are due to Cl-H contacts with $d_i + d_e \approx 2.8$ Å. C-H, Cl-H, and O-H contacts contribute about 18.9%, 18.2%, and 5.7% respectively to the total Hirshfeld surface area.

3.6. Shape index, curvedness, and electrostatic potential map

In order to get more details about Hirshfeld surface and the molecular packing in the crystal other properties like shape index, curvedness and electrostatic potential map were studied.

The molecular Hirshfeld surface mapping over the shape index of the compound is presented in Figure 7(a). This map is used to identify the complementary bumps (blue) and hollows (red) where two molecular Hirshfeld surfaces touch each other [28]. The red and blue color regions on the shape index map represent the cluster of the surface about the acceptor and the donor atoms respectively.

Figure 7(b) shows curvedness map. It is the large green region separated by dark blue curves. The sharp curvature areas correspond to high values of curvedness, while the flat areas of the surface correspond to low values of curvedness. From this map, it is clear that there is no planar stacking between the molecules.

The electrostatic potential mapping in Hirshfeld surface of the molecule shown in Figure 7(c).

On this map, the red color regions are around hydrogen bond acceptor (electronegative regions); the blue color regions are around hydrogen bond donor (electropositive regions) [29]. For the compound (**4**) electronegative regions around N13 atom and electropositive regions around C10-H10A atoms.

3.7. Energy frameworks

Energy frameworks is a powerful method to understand the crystal packing of molecules by studying the different interaction energies, and to know the dominant among them. Energy frameworks calculations were performed by employing CrystalExplorer-17 software [26] with B3LYP function and 6-31G (d, p) basis set within a radius of 3.8 Å around a single molecule.

Table 6 lists the diffrent interaction energies such as electrostatic, polarization, dispersion, and repulsion between the molecular pairs. R is the mean atomic distance between molecular centroids in Å. The scale factors used for the construction of energy framework for B3LYP/6-31G (d,p) electron densities are k_ele = 1.057, k_pol = 0.740, k_disp = 0.871, k_rep = 0.618 [30]. The calculated interaction energies for electrostatic, polarization, dispersion, repulsion and total energy are -66.0 kJ/mol, -21.1 kJ/mol, -224.3 kJ/mol, 144.5 kJ/mol and -191.6 kJ/mol respectively. The dispersion energy is the dominant of all the interaction energies. Figure 8 represents the visualization of different interaction energies like Coulomb interaction energy (red), dispersion energy (green), total interaction energy (blue) of the compound along several axes. The cylinders in the energy framework represent the rel-

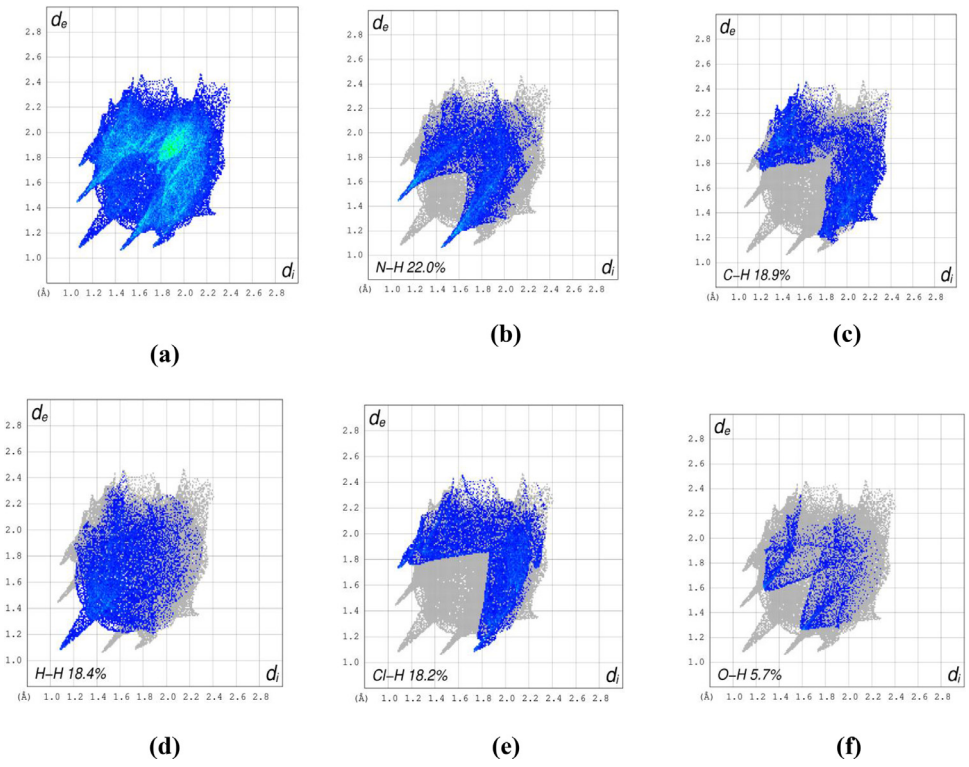

Fig. 6. Fingerprint plots of the compound a) From all the contacts b) Decomposed fingerprint plot showing N-H (22.0%) contacts c) C-H (18.9%) contacts d) H-H (18.4%) contacts e) Cl-H (18.2%) contacts f) O-H (5.7%) contacts.

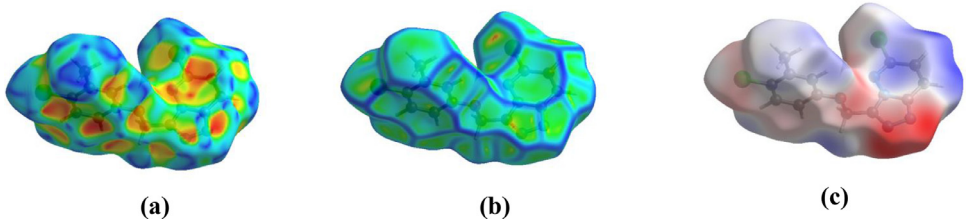

Fig. 7. Hirshfeld surface with (a) shape index, (b) curvedness and (c) electrostatic potential map.

Table 6
Different interaction energies of the molecular pairs in kJ/mol.

	N	Symmetry operation	R (Å)	Electron density	E_ele	E_pol	E_dis	E_rep	E_tot
	1	-x, -y, -z	6.67	B3LYP/6-31G(d,p)	-3.7	-1.2	-54.5	35.7	-30.2
	2	x, y, z	6.13	B3LYP/6-31G(d,p)	-19.1	-4.8	-36.9	30.9	-36.9
	2	x, -y+1/2, z+1/2	10.81	B3LYP/6-31G(d,p)	-5.3	-1.0	-4.9	2.5	-9.0
	1	-x, -y, -z	7.61	B3LYP/6-31G(d,p)	1.5	-1.4	-13.3	3.1	-9.2
	2	-x, y+1/2, -z+1/2	11.02	B3LYP/6-31G(d,p)	-5.5	-0.7	-14.5	14.7	-9.9
	2	x, -y+1/2, z+1/2	8.93	B3LYP/6-31G(d,p)	-9.9	-1.6	-18.9	12.6	-20.3
	2	-x, y+1/2, -z+1/2	10.65	B3LYP/6-31G(d,p)	-6.4	-2.2	-18.5	11.1	-17.7
	1	-x, -y, -z	6.08	B3LYP/6-31G(d,p)	-6.7	-1.7	-40.7	20.4	-31.2
	1	-x, -y, -z	7.04	B3LYP/6-31G(d,p)	-10.9	-6.5	-22.1	13.5	-27.2

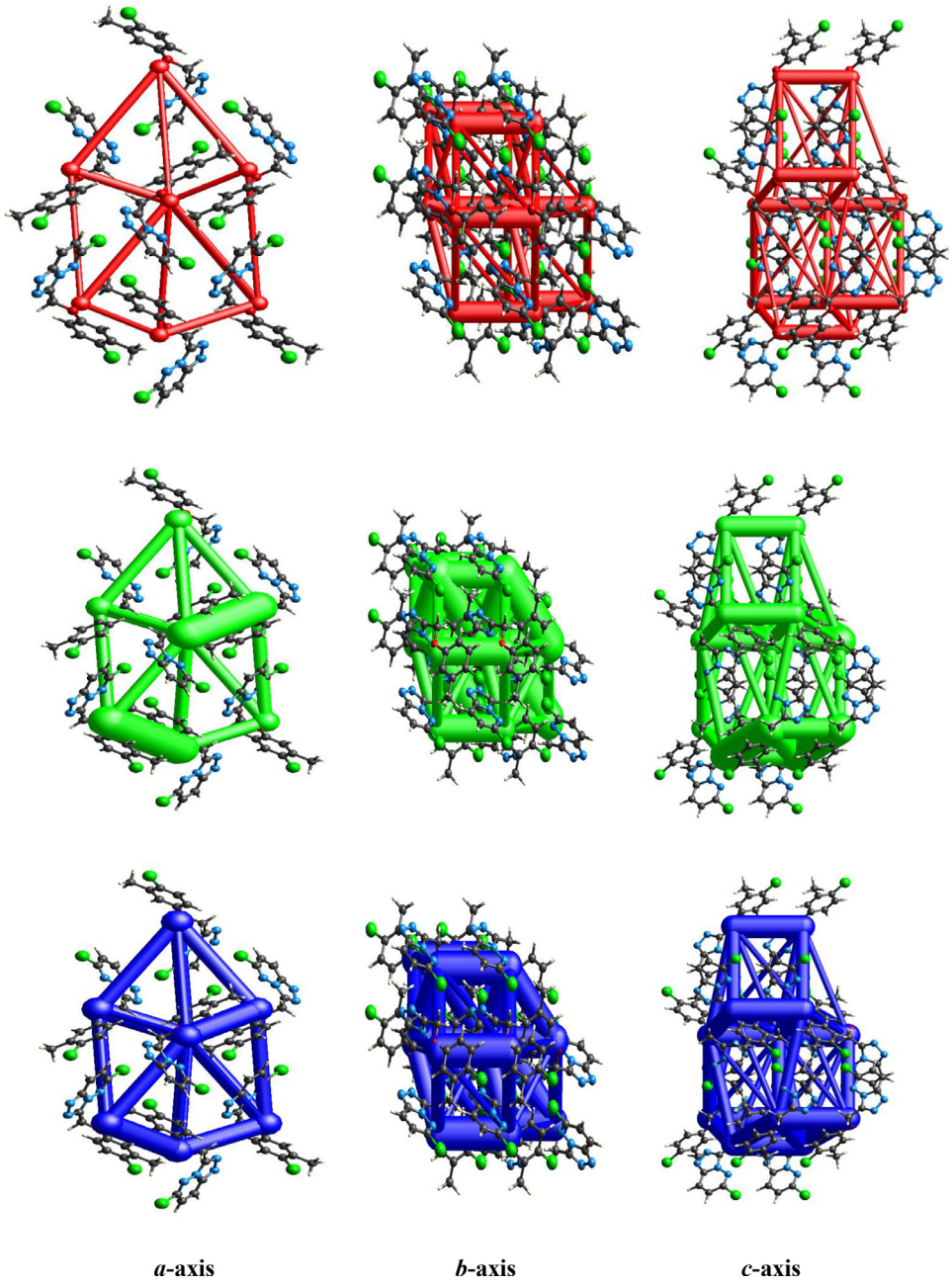

Fig. 8. The graphical representation of electrostatic interactions (Coulomb interaction energy (red), dispersion energy (green), total interaction energy (blue) of the compound along different axes.

ative strengths of molecular packing in *a*, *b*, and *c* directions. An overall scale factor is applied in order to contract or expand the size of the cylinders in the framework [31].

4. Conclusions

The Triazolo pyridine derivative was synthesized and characterized using different methods to identify the final structure. DFT calculations for the title compound show very good agreements between the predicted and the experimental values. The small energy gap (3.469 eV) between (HOMO-LUMO) indicates a soft molecule and higher chemical reactivity. The structure is reinforced by C-H...N intermolecular interactions and C-Cl...cg interactions. Hirshfeld surface studies show that the major contribution is from N-H contacts with 22%. Energy frameworks calculations show that the dispersion energy is the dominant factor among all interaction energies.

Author Statement

All authors have contributed in preparation of the manuscript. **Hamdi Hamid Sallam**: Analysis and interpretation of the data, calculations, visualization, conceptualization, methodology, and writing-original draft. **Yasser Hussien Eissa Mohammed** and **Fares Hezam Al-Ostoot:** Synthesis, spectroscopic characterizations, methodology, visualization and writing-original chemistry manuscript draft. **Sridhar M. A.**: Investigation, supervision, and approval of the final version. **Shaukath Ara Khanum**: Synthesis, spectroscopic characterizations.

Declaration of Competing Interest

The authors declare that they have no known competing financial interests or personal relationships that could have appeared to influence the work reported in this paper.

This manuscript has not been submitted to, nor is under review at, another journal or other publishing venue.

The authors have no affiliation with any organization with a direct or indirect financial interest in the subject matter discussed in the manuscript.

Acknowledgments

Hamdi Hamid Sallam is thankful to the Taiz University, Yemen, Yasser Hussein Eissa Mohammed is thankful to the University of Hajjah, Yemen and Fares Hezam Al-Ostoot is thankful to the Al-Baydha University, Yemen, and also to the Government of Yemen for providing financial assistance under the teacher's fellowship. Shaukath Ara Khanum thankfully acknowledges the financial support provided by VGST, Bangalore, under CISEE Program [Project sanction order: No.VGST/CISEE/282/2012-13]. All the authors are grateful to the University of Mysore, Mysuru, India for providing laboratory facilities to carry out the research work and to SAIF, IIT Madras, for collecting single crystal X-ray diffraction data.

Supplementary materials

Supplementary material associated with this article can be found, in the online version, at doi:10.1016/j.molstruc.2021.130282.

References

[1] B. Schulze, U.S. Schubert, Beyond click chemistry–supramolecular interactions of 1, 2, 3-triazoles, Chemical Society Reviews 43 (2014) 2522–2571.
[2] M. Verma, V. Luxami, K. Paul, Synthesis of new 2, 3-disubstituted pyridines containing a 1, 2, 3-triazole in the side-chain via one-pot copper-catalyzed azide-alkyne cycloaddition, ARKIVOC (7) (2015) 28–41.
[3] S.J. Dabade, D. Mandloi, A.V. Bajaj, A. Thakur, In silico evaluation of inhibitory potential of novel triazole derivatives against therapeutic target myristoyl-CoA: protein N-myristoyltransferase (NMT) of Candida albicans, Network Modeling Analysis in Health Informatics and Bioinformatics 9 (2020) 1–17.
[4] A. Diaz-Ortiz, P. Prieto, J.R Carrillo, R. Martin, I. Torres, Applications of metal-free 1, 2, 4-triazole derivatives in materials science, Current Organic Chemistry 19 (2015) 568–584.
[5] Y.M. Ali, M.F. Ismail, F.S. Abu El-Azm, M.I. Marzouk, Design, synthesis, and pharmacological assay of novel compounds based on pyridazine moiety as potential antitumor agents, Journal of Heterocyclic Chemistry 56 (2019) 2580–2591.
[6] E.M. Ahmed, M.S. Hassan, A.A. El-Malah, A.E. Kassab, New pyridazine derivatives as selective COX-2 inhibitors and potential anti-inflammatory agents; design, synthesis and biological evaluation, Bioorganic chemistry 95 (2020) 103497.
[7] A.A. Abu-Hashem, U. Fathy, M.A. Gouda, Synthesis of 1, 2, 4-triazolopyridazines, isoxazolofuropyridazines, and tetrazolopyridazines as antimicrobial agents, Journal of Heterocyclic Chemistry 57 (2020) 3461–3474.
[8] J.M. Contreras, Y.M. Rival, S. Chayer, J.J. Bourguignon, C.G. Wermuth, Aminopyridazines as acetylcholinesterase inhibitors, Journal of medicinal chemistry 42 (1999) 730–741.
[9] Q. Xu, Y. Wang, J. Xu, M. Sun, H. Tian, D. Zuo, Q. Guan, K. Bao, Y. Wu, W. Zhang, Synthesis and bioevaluation of 3, 6-diaryl-[1, 2, 4] triazolo [4, 3-b] pyridazines as antitubulin agents, ACS medicinal chemistry letters 7 (2016) 1202–1206.
[10] A.A.M. El-Reedy, N.K. Soliman, Synthesis, biological activity and molecular modeling study of novel 1, 2, 4-triazolo [4, 3-b][1, 2, 4, 5] tetrazines and 1, 2, 4-triazolo [4, 3-b][1, 2, 4] triazines, Scientific Reports 10 (2020) 1–18.
[11] L.P. Guan, X. Sui, X.Q. Deng, Y.C. Quan, Z.S. Quan, Synthesis and anticonvulsant activity of a new 6-alkoxy-[1, 2, 4] triazolo [4, 3-b] pyridazine, European journal of medicinal chemistry 45 (2010) 1746–1752.
[12] C.H. Park, D. Kim, H. Jung, J.H. Jeon, R. Achary, J.Y. Lee, P. Kim, H. Jung, J.Y. Hwang, D.H. Ryu, J.Du Ha, S.Y. Cho, Design and Synthesis of Novel 3-(2-Aminopyridin-3-yl)-1, 2, 4-Triazolo [4, 3-b] Pyridazine Derivatives as a Reversible Bruton's Tyrosine Kinase Inhibitors, Bulletin of the Korean Chemical Society 39 (2018) 853–857.
[13] K. Mogilaiah, G.R. Reddy, Chloramine-T mediated synthesis of 1, 2, 4-triazolo[4, 3-a][1, 8] naphthyridines under microwave irradiation, Journal of Chemical Research 2 (2004) 145–147.
[14] F.H. Al-Ostoot, D.V. Geetha, Y.H.E. Mohammed, P. Akhileshwari, M.A. Sridhar, S.A. Khanum, Design-based synthesis, molecular docking analysis of an anti-inflammatory drug, and geometrical optimization and interaction energy studies of an indole acetamide derivative, Journal of Molecular Structure 1202 (2020) 127244.
[15] D.V. Geetha, F.H. Al-Ostoot, Y.H.E. Mohammed, M.A. Sridhar, S.A. Khanum, N.K. Lokanath, Synthesis, Elucidation, Hirshfeld surface analysis, and DFT calculations of 4-chloro-N-[2-(2-1H-indol-3-yl-acetylamino)-phenyl]-benzamide, Journal of Molecular Structure 1178 (2019) 384–393.
[16] H.A. Khamees, Y.H.E. Mohammed, S. Ananda, F.H. Al-Ostoot, Y. Sangappa, S. Alghamdi, S.A. Khanum, M. Madegowda, Effect of o-difluoro and p-methyl substituents on the structure, optical properties and anti-inflammatory activity of phenoxy thiazole acetamide derivatives: Theoretical and experimental studies, Journal of Molecular Structure 1199 (2020) 127024.
[17] L. Krause, R. Herbst-Irmer, G.M. Sheldrick, D. Stalke, Comparison of silver and molybdenum microfocus X-ray sources for single-crystal structure determination, Journal of applied crystallography 48 (2015) 3–10.
[18] A. P. E. X. Bruker, and A. X. S. Saint, Inc., Search PubMed;(b) GM Sheldrick, Acta Crystallographica, Section. A 64 (2008) 112.
[19] G.M. Sheldrick, Crystal structure refinement with SHELXL, Acta Crystallographica Section C: Structural Chemistry 71 (2015) 3–8.
[20] A.L. Spek, PLATON, an integrated tool for the analysis of the results of a single crystal structure determination, Acta Crystallographica A 46 (1990) c34.
[21] C.F. Macrae, I.J. Bruno, J.A. Chisholm, P.R. Edgington, P. McCabe, E. Pidcock, L. Rodriguez-Monge, R. Taylor, J. van de Streek, P.A. Wood, Mercury CSD 2.0–new features for the visualization and investigation of crystal structures, Journal of Applied Crystallography 41 (2008) 466–470.
[22] M.J. Frisch, G.W. Trucks, H.B. Schlegel, G.E. Scuseria, M.A. Robb, J.R. Cheeseman, G. Scalmani, V. Barone, B. Mennucci, G.A. Petersson, H. Nakatsuji, M. Caricato, X. Li, H.P. Hratchian, A.F. Izmaylov, J. Bloino, G. Zheng, J.L. Sonnenberg, M. Hada, M. Ehara, K. Toyota, R. Fukuda, J. Hasegawa, M. Ishida, T. Nakajima, Y. Honda, O. Kitao, H. Nakai, T. Vreven, J.A. Montgomery Jr., J.E. Peralta, F. Ogliaro, M. Bearpark, J.J. Heyd, E. Brothers, K.N. Kudin, V.N. Staroverov, R. Kobayashi, J. Normand, K. Raghavachari, A. Rendell, J.C. Burant, S.S. Iyengar, J. Tomasi, M. Cossi, N. Rega, J.M. Millam, M. Klene, J.E. Knox, J.B. Cross, V. Bakken, C. Adamo, J. Jaramillo, R. Gomperts, R.E. Stratmann, O. Yazyev, A.J. Austin, R. Cammi, C. Pomelli, J.W. Ochterski, R.L. Martin, K. Morokuma, V.G. Zakrzewski, G.A. Voth, P. Salvador, J.J. Dannenberg, S. Dapprich, A.D. Daniels, O. Farkas, J.B. Foresman, J.V. Ortiz, J. Cioslowski, D.J. Fox, Gaussian 09, Revision A.02, Gaussian Inc., Wallingford CT, 2009.
[23] V.N. Badavath, A. Kumar, P.K. Samanta, S. Maji, A. Das, G. Blum, A. Jha, A. Sen, Determination of potential inhibitors based on isatin derivatives against SARS–CoV-2 main protease (mpro): a molecular docking, molecular dynamics and structure-activity relationship studies, Journal of Biomolecular Structure and Dynamics (2020) 1–19.
[24] J.I. Aihara, Weighted HOMO-LUMO energy separation as an index of kinetic stability for fullerenes, Theoretical Chemistry Accounts 102 (1999) 134–138.
[25] V.K. Singh, S.K. Verma, R. Kadu, S.M. Mobin, Identification of unusual C–Cl$\cdots\pi$ contacts in 2-(alkylamino)-3-chloro-1, 4-naphthoquinones: effect of N-substituents on crystal packing, fluorescence, redox and anti-microbial properties, RSC Advances 5 (2015) 43669–43686.
[26] M.A. Spackman, D. Jayatilaka, Hirshfeld surface analysis, Crystal *Engineering Communications* 11 (2009) 19–32.
[27] J.J. McKinnon, D. Jayatilaka, M.A. Spackman, Towards quantitative analysis of intermolecular interactions with Hirshfeld surfaces, Chemical Communications 37 (2007) 3814–3816.
[28] J.J. McKinnon, M.A. Spackman, A.S. Mitchell, Novel tools for visualizing and exploring intermolecular interactions in molecular crystals, Acta Crystallographica Section B: Structural Science 60 (2004) 627–668.
[29] M.J. Turner, S. Grabowsky, D. Jayatilaka, M.A. Spackman, Accurate and efficient model energies for exploring intermolecular interactions in molecular crystals, The journal of physical chemistry letters 5 (2014) 4249–4255.
[30] C.F. Mackenzie, P.R. Spackman, D. Jayatilaka, M.A. Spackman, CrystalExplorer model energies and energy frameworks: extension to metal coordination compounds, organic salts, solvates and open-shell systems, International Union of Crystallography Journal 4 (2017) 575–587.
[31] A.J. Edwards, C.F. Mackenzie, P.R. Spackman, D. Jayatilaka, M.A. Spackman, Intermolecular interactions in molecular crystals: what's in a name? Faraday Discussions 203 (2017) 93–112.